ORIGINAL PAPER

A carbothermal reduction method for enhancing the electrochemical performance of LiFePO$_4$/C composite cathode materials

Shaoying Weng · Zeheng Yang · Qiang Wang ·
Jun Zhang · Weixin Zhang

Abstract LiFePO$_4$/C composite cathode material has been synthesized by a carbothermal reduction method using β-FeOOH nanorods as raw materials and glucose as both reducing agent and carbon source. The results indicate that the content of carbon and the morphology of raw material have effect on the electrochemical performance of the final LiFePO$_4$/C material. Sample LFP14 with a carbon content of 2.79 wt.% can deliver discharge capacities of 158.8, 144.3, 111.0, and 92.9 mAh g^{-1} at 0.1, 1, 10, and 15 C, respectively. When decreasing the current from 15 C back to 0.1 C, a discharge capacity of 157.5 mAh g^{-1} is recovered, which is 99.2 % of its initial capacity. Therefore, as a kind of cathode material for lithium ion batteries, this LiFePO$_4$/C material synthesized via a carbothermal reduction method is promising in large-scale production, and has potential application in upcoming hybrid electric vehicles or electric vehicles.

Keywords Lithium ion batteries · Lithium iron phosphate · Carbothermal reduction method · Carbon coating · Electrochemical performance

S. Weng · Z. Yang (✉) · Q. Wang · J. Zhang · W. Zhang
School of Chemical Engineering, Hefei University of Technology,
Hefei, Anhui 230009, People's Republic of China
e-mail: yangzh0219@sina.com

S. Weng · Z. Yang · Q. Wang · J. Zhang · W. Zhang
Anhui Key Laboratory of Controllable
Chemical Reaction & Material Chemical Engineering,
Hefei, Anhui 230009, People's Republic of China

Introduction

Over the last decade, the demand for electrochemical energy storage systems with high capacity and high power grows at an unprecedented high speed. Lithium ion batteries which exhibit high energy and high power density seemingly could be one of the best solutions for these systems [1–3]. Since olivine-type lithium iron phosphate (LiFePO$_4$) was firstly reported as cathode electrode material for rechargeable lithium ion batteries in 1997 [4], it has received extensive studies as a promising cathode material for lithium ion batteries in applications such as the upcoming hybrid electric vehicles (HEVs) or electric vehicles (EVs), owing to its low cost, nontoxicity, environment benignity, cycling stability, high theoretical capacity (170 mAh g^{-1}) and a stable charge–discharge potential (3.45 V versus Li$^+$/Li).

Nevertheless, the main disadvantages of LiFePO$_4$ material are its poor electronic conductivity [5] and slow lithium ion diffusion [6] due to a separation of FeO$_6$ octahedral by PO$_4^{3-}$ in the LiFePO$_4$ structure and a slightly distorted hexagonal close-packed oxygen array [7]. In order to enhance the electrochemical properties of LiFePO$_4$, various strategies have been adopted to modify the material, such as doping with supervalent cations [8, 9], coating with conductive materials [10], and reducing the particle sizes [11, 12]. In recent years, coating with conductive layer and controlling the particle size [13] have stood out as reliable methods to modify LiFePO$_4$. The conductive layer coated on particle surfaces can improve the electronic conductivity of LiFePO$_4$, and it also acts as dispersive media among the particles to prevent the particles growth [14]. Reducing the particle size is an effective way to decrease the diffusion distance for charge transfer, which can overcome the low Li ion diffusion rate [15].

Currently, various methods have been developed to prepare LiFePO$_4$/C composite for enhancing its electrochemical

performance, such as co-precipitation [13], sol–gel method [16], spray technology [17], hydrothermal/solvothermal synthesis [18, 19], and solid-state reaction [20–23]. Excluding solid-state reaction, many obstacles have been encountered for the other methods when performing mass production, since the synthesis techniques are complicated and the synthesis conditions are hard to control for those methods. Solid-state reaction is still the better choice for commercial production of $LiFePO_4$. However, some shortcomings of the traditional solid-state reaction method, such as high-energy consumption, poor product uniformity, oxidation of Fe (II), impurities occurring, and high value of raw materials, were reported in previous research works [11]. To overcome these shortcomings, carbothermal reduction method has been adopted as an alternative way to replace the widely used traditional solid-state reaction method.

Carbothermal reduction method has been considered as a convenient and energy-efficient method in recent reports to synthesize $LiFePO_4/C$ composite from inexpensive Fe^{3+} precursors such as cheap $FePO_4$ [24–26] and Fe_2O_3 [27]. Wang et al. [25] reported that a core-shell $LiFePO_4/C$ composite prepared by carbothermal reduction method combined with an in situ polymerization restriction method could exhibit a capacity of 168 mAh g^{-1} at charge/discharge rates of 0.6 C (0.1 A g^{-1}) and a capacity of 90 mAh g^{-1} at 60 C (10 A g^{-1}). Sun et al. [27] used nano-ferric oxide as iron source and polyacene (PAS) as reductive agent and high conductive carbon source by carbothermal reduction method to synthesize the $LiFePO_4/C$. The first cycle discharge capacity at 0.2 C rate was 159.7 mAh g^{-1}, and the discharge capacity had almost no decrease over 100 cycles. Yang et al. [28] synthesized $LiFePO_4/C$ composite using FeOOH, LiH_2PO_4 and PF resin as raw materials, and studied the influence of sintering temperature on electrochemical properties of the product. The $LiFePO_4/C$ composite prepared at 750 °C exhibited the best electrochemical performance. The initial capacity of 158 mAh g^{-1} was obtained at 0.2 C and capacities of 136, 131 and 118 mAh g^{-1} could still be delivered at the rate of 1, 2, and 10 C, respectively. Polymer additives were used as carbon sources in these reported carbothermal reduction methods.

Herein, we choose inexpensive and abundant β-FeOOH nanorods as raw materials and glucose as both reducing agent and carbon source to prepare $LiFePO_4/C$ composites (300–400 nm) through a carbothermal reduction method with lower sintering temperature and shorter reaction time. The β-FeOOH nanorods extensively used in the production of pigment, catalysts, and raw materials of hard and soft magnets were prepared by hydrolysis process. Glucose acted as both reducing agent and carbonaceous coating conductor source. In addition, glucose also acted as dispersive media among the particles to prevent the particles from growing. The $LiFePO_4/C$ composites with appropriate

carbon content exhibit an excellent electrochemical performance at high rate.

Experimental

All chemicals were purchased from China and used as raw materials without further purification.

Synthesis of β-FeOOH nanorods

β-FeOOH nanorods were prepared by hydrolysis process. In a typical experiment, 1.012 g of $FeCl_3 \cdot 6H_2O$ (AR, Shanghai Chemical Reagents Corporation, China) was dissolved in 25 mL of distilled water at room temperature and then, the solution was heated at 95 °C for about 12 h in air. During the reaction, $FeCl_3$ slowly hydrolyzed and a yellow precipitation took place progressively. After the reaction, the precipitated products were filtered, washed sequentially with deionized water and ethanol to remove the residue chloride ions and other remnants. The obtained yellow powder was subsequently dried at 70 °C in air.

Synthesis of $LiFePO_4/C$ composites via a carbothermal reduction method

The $LiFePO_4/C$ composites were prepared using the as-synthesized β-FeOOH nanorods as a Fe(III) raw material. A stoichiometric mixture of starting materials lithium dihydrogen phosphate (LiH_2PO_4, AR, Shanghai Chemical Reagents Corporation, China), the as-synthesized β-FeOOH nanorods and lithium carbonate (Li_2CO_3, AR, Shanghai Chemical Reagents Corporation, China) in a molar ratio of 1:1:0.025 were placed in a 50-mL Teflon milling vessel. The desired amount of glucose ($C_6H_{12}O_6$, AR, Shanghai Chemical Reagents Corporation, China) was also added. Glucose was used as reduction agent to convert Fe (III) to Fe(II) during the reaction, and the precursor of carbon coating on $LiFePO_4$ particles. About 2.5 atom% excess Li_2CO_3 was added with an initial expectation to compensate for the loss of Li_2O during next heating step. Glucose was added in proportions of 7, 10, 14, 17, and 21 wt.% with respect to the theoretical weight of $LiFePO_4$ product which was calculated based on the molar weight of Fe in the raw material β-FeOOH. Finally, the mixture was added into a Teflon milling vessel and kept ball-milled for 6 h with ethanol as the milling medium. After the evaporation of ethanol, the obtained precursor was heated at 350 °C for 4 h and then at 650 °C for 9 h in N_2 atmosphere to obtain $LiFePO_4/C$ composites.

The $LiFePO_4/C$ composites prepared with the addition of 7, 10, 14, 17, and 21 wt.% of glucose were named as LFP7, LFP10, LFP14, LFP17, and LFP21, respectively.

Characterization of the samples

The composition and phase purity of the prepared samples were examined by X-ray powder diffraction (XRD) patterns taken on a Rigaku D/max-r B X-ray diffractometer with Cu Kα radiation (λ=1.5418 Å), operated at 40 kV and 80 mA. Field-emission scanning electron microscopy (FESEM) measurement was carried out on a FEI Siron 200 field-emission scanning electron microscope, operated at an acceleration voltage of 10 kV. Transmission electron microscopy (TEM) images were taken on a Hitachi H-800 transmission electron microscope. High-resolution transmission electron microscopic (HRTEM) images were taken on a Philips CM 20 FEG transmission electron microscope, operated at an accelerating voltage of 200 kV. The carbon content in the samples was measured by a Carbon Sulfur Automatic Analyzer (HH2000A, Wuxi Chuangxiang Co. China).

Electrochemical measurements

The electrodes for electrochemical studies were prepared by mixing 80 wt.% active material of LiFePO$_4$/C, 15 wt.% conducting carbon black, and 5 wt.% polyvinylidene fluoride as a binder in a solvent of N-methyl-2-pyrrolidone (NMP) to form a homogeneous slurry. Then, the mixed slurry was cast onto an aluminum foil with the slurry thickness controlled. After the evaporation of the solvent at 65 °C for 4 h in air, the cathode was roll-pressed and cut into pellets of required size for coin-cell fabrication, then the pellets were further dried under high vacuum at 120 °C for 5 h. Lithium metal foil (Energy Lithium Limited Corporation, China) was used as the anode. The liquid electrolyte used was 1 M solution of LiPF$_6$ in ethylene carbonate/diethyl carbonate (EC/DEC, 1:1 v/v), and the separator was a polypropylene membrane with micro-pores (Celgard 2400). The coin-type cells (CR2032) were assembled in an argon-filled glove box (oxygen and water contents below 2 and 0.5 ppm, respectively). The galvanostatical charge–discharge experiment was performed at different current rates (1 C=170 mA g^{-1}) between 2.5 and 4.2 V at room temperature using a multi-channel battery tester (Neware Battery Testing System, Shenzhen Neware Electronic Co., China). Cyclic voltammetry (CV) and electrochemical impedance spectroscopic (EIS) measurements were performed at room temperature on a CHI604C electrochemical workstation (Shanghai Chenhua Instrument Co. Ltd) controlled by a personal computer. Cyclic voltammetry was performed at a scan rate of 0.1 mV s^{-1} from 2.5 to 4.2 V (versus Li$^+$/Li), and in electrochemical impedance spectroscopic measurements, the excitation potential applied to the cells was 5 mV and the frequency ranged from 100 kHz to 10 mHz.
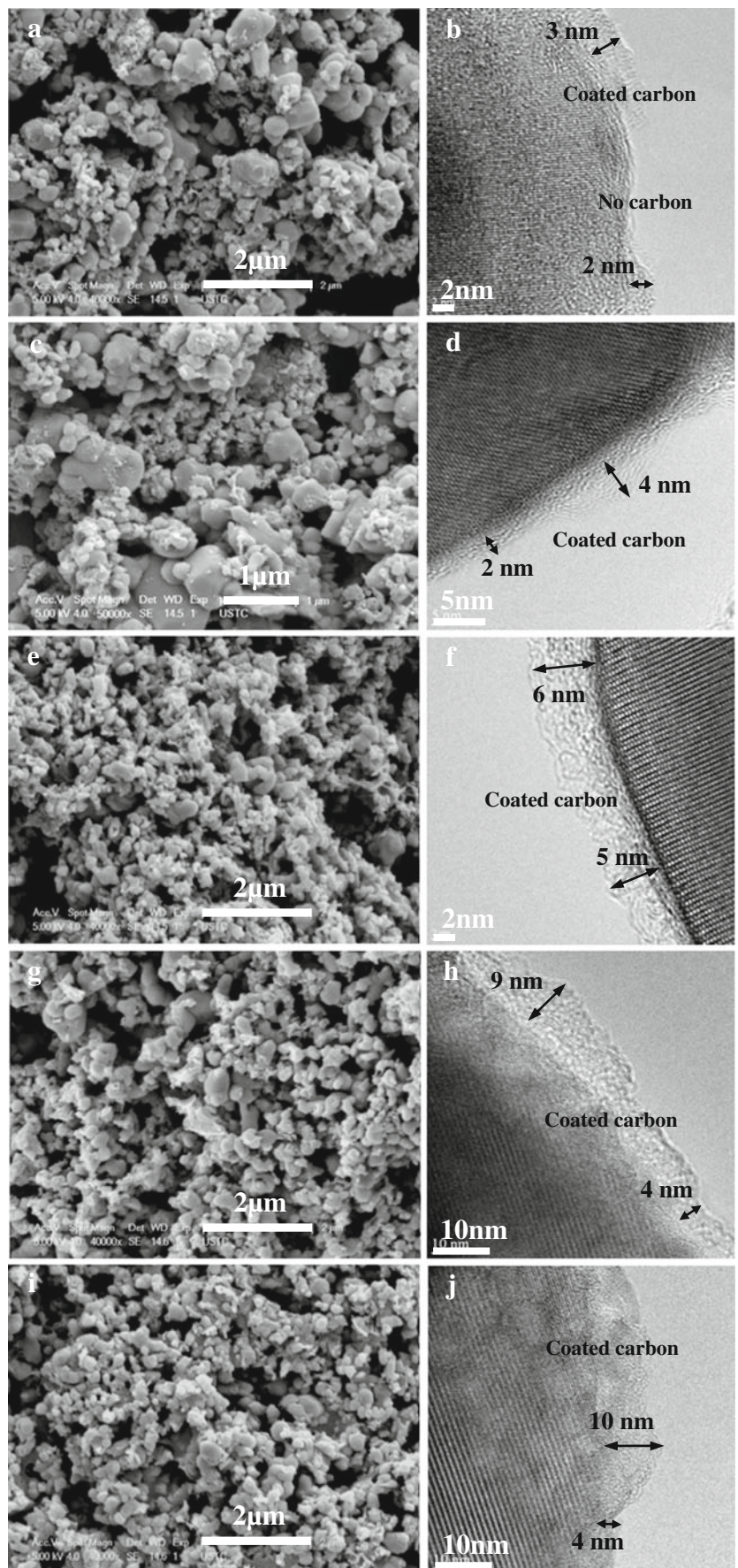
Results and discussion

Figure 1 shows the composition, structure, and morphology of the product which was prepared by hydrolysis of FeCl$_3$ in water at 95 °C for 12 h. The XRD pattern in Fig. 1a indicates that all the diffraction peaks can be indexed to tetragonal β-FeOOH with I4/m space group (JCPDS No. 34-1266). No obvious impurity peaks are detected. Figure 1b presents the low-magnification TEM image of β-FeOOH. It can be seen that this β-FeOOH sample is entirely composed of uniform nanorods with good mono-dispersity. Figure 1c shows that β-FeOOH nanorods have an average diameter of 90 nm and an average length of 600 nm.

Figure 2 shows the XRD patterns of samples LFP7, LFP10, LFP14, LFP17, and LFP21 synthesized using the as-synthesized β-FeOOH nanorods as Fe(III) raw materials and different amount of glucose as carbon source by the carbothermal reduction method, respectively. All the diffraction peaks can be indexed to orthorhombic LiFePO$_4$ with Pnma space group (JCPDS card No. 83-2092) without any obvious impurities detected. Note that there is no additional diffraction peaks associated with carbon generated from glucose pyrolysis under high temperature, which indicates that the carbon is amorphous and its presence does not influence the structure of LiFePO$_4$.

The coated carbon content of the LiFePO$_4$/C composites was measured by a Carbon Sulfur Automatic Analyzer (HH2000A, Wuxi Chuangxiang Co. China). The results indicate that the coated carbon contents of samples LFP7, LFP10, LFP14, LFP17, and LFP21 are 0.99, 1.85, 2.79, 3.60, and 4.48 wt.%, respectively. The carbon content of the LiFePO$_4$/C composites increases with the increased amount of glucose. Fig. S1a–e presents the TEM images of samples LFP7, LFP10, LFP14, LFP17, and LFP21. It can be seen that the particle sizes of samples LFP7, LFP10, LFP14, LFP17, and LFP21 are about 400–700 nm, 300–600 nm, 300–400 nm, 300–400 nm, and 300–400 nm, respectively. As shown in Fig. S1a–e, with the increase of carbon content, a significant decrease of particle size and a more uniform particle size distribution are observed. For this phenomenon, the reason is that there is not enough glucose to coat on the precursor during the preparation of sample LFP7, so it has the largest particle size and the widest particle size distribution. However, during the preparation of samples LFP14, LFP17, and LFP21, there is enough glucose to coat on the precursor, so the particle size and particle size distribution for these samples are similar. It is clear that glucose could prevent the particles from growing.

FESEM images in Fig. 3 show that LiFePO$_4$/C composites are composed of particles. The particle sizes of samples LFP7 (Fig. 3a), LFP10 (Fig. 3c), LFP14 (Fig. 3e), LFP17 (Fig. 3g), and LFP21 (Fig. 3i) are about 400–700 nm, 300–

Fig. 1 XRD pattern (**a**) and TEM images (**b**, **c**) of β-FeOOH prepared from hydrolysis process

600 nm, 300–400 nm, 300–400 nm, and 300–400 nm, respectively, which are in good agreement with the TEM results. For further insight into the microstructure of samples LFP7, LFP10, LFP14, LFP17, and LFP21, HRTEM observations were carried out and the results are also shown in Fig. 3b, d, f, h, j. Figure 3b shows that the amorphous carbon cannot cover all over the particle, thus sample LFP7 has a non-uniform carbon coating. And for sample LFP10, although the carbon has almost covered over the particle, the carbon layer is too thin and non-uniform (as shown in Fig. 3d). Figure 3f shows that sample LFP14 has been coated with a uniform and thin carbon layer (about 5–6 nm) on the surface of the particle. As for samples LFP17 and LFP21, Fig. 3h and j present that the particle surfaces have been coated completely by carbon layer. However, the coated carbon layers are thick and rough (about 4–9 nm and 4–10 nm, respectively). It is believed that sample LFP14 has an optimal glucose distribution to inhibit the particle growth, and the particle is coated by a uniform carbon layer.

Although the carbothermal reduction reaction is a solid-state reaction, the morphology of the LiFePO$_4$/C composite samples indicates that the present method can avoid the disadvantages of wide particle size distribution and some

impurities such as Li$_3$PO$_4$, Fe$_2$O$_3$, and Li$_3$Fe$_2$(PO$_4$)$_3$, which normally happen to the final product due to inhomogeneity of the reagents in solid-state reaction. The reason mainly results from uniform β-FeOOH nanorods as Fe(III) raw materials and appropriate glucose as the carbon source which can effectively control the particle size and size distribution.

The initial charge–discharge profiles of samples LFP7, LFP10, LFP14, LFP17, and LFP21 at 0.1 C between 2.5 and 4.2 V are shown in Fig. 4. The charge–discharge curves for all the samples are similar, with flat plateaus corresponding to the lithium extraction and insertion reactions, but they vary in plateau potentials. The charge–discharge potential plateaus are 3.47–3.38 V for LFP7, 3.46–3.38 V for LFP10, 3.45–3.40 V for LFP14, 3.45–3.40 V for LFP17, and 3.46–3.40 V for LFP21. The lowest electrochemical polarization of sample LFP14 (shown in the inset of Fig. 4) suggests that the increased conductivity is induced by reducing the particle sizes and coating appropriate carbon layers. And the discharge capacities of samples LFP7, LFP10, LFP14, LFP17, and LFP21 are 150.5, 152.1, 158.8, 156.6, and 154.1 mAh g^{-1} at 0.1 C, respectively, indicating that the discharge capacities of the samples increase firstly, and then decrease with the increased carbon content.

Based on the results above, we chose samples LFP7, LFP14, and LFP21 to further study their rate capabilities and cycling performances. Figure 5a–c shows the initial charge–discharge profiles between 2.5 and 4.2 V at room temperature with current density varying from 0.1 C (17 mA g^{-1}) to 15 C (2,550 mA g^{-1}). The discharge capacities and the plateau voltage differences between charge and discharge are similar for samples LFP7, LFP14, and LFP21 at 0.1 C. While the discharge rate increases to 1 C, their discharge capacities are 93.9, 144.3, and 135.0 mAh g^{-1}, respectively. And the charge–discharge plateau potentials of samples LFP7, LFP14, and LFP21 are 3.64–2.99 V, 3.47–3.36 V and 3.48–3.35 V, respectively. A huge polarization and a fast capacity fading are observed for sample LFP7 when the discharge rate increases to 1 C, but this situation

Fig. 2 XRD patterns of samples LFP7 (**a**), LFP10 (**b**), LFP14 (**c**), LFP17 (**d**), and LFP21 (**e**)

Fig. 3 FESEM and HRTEM images of samples LFP7 (**a**, **b**), LFP10 (**c**, **d**), LFP14 (**e**, **f**), LFP17 (**g**, **h**), and LFP21 (**i**, **j**)
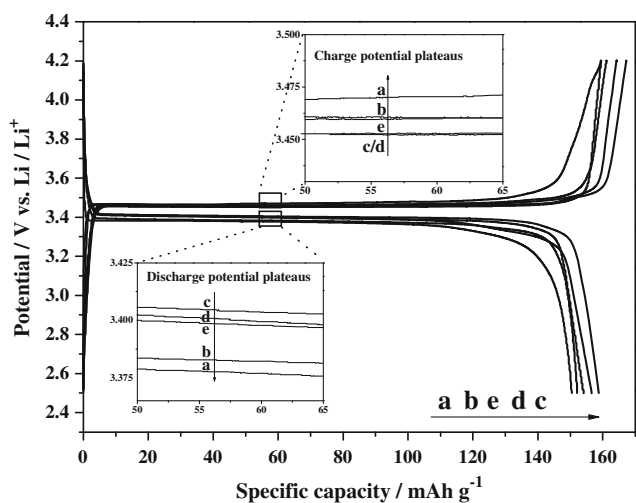
Fig. 4 Initial charge–discharge profiles of samples LFP7 (**a**), LFP10 (**b**), LFP14 (**c**), LFP17 (**d**), and LFP21 (**e**) at 0.1 C

does not happen to samples LFP14 and LFP21. Sample LFP14 has the least plateau voltage difference and the highest discharge capacity. When the discharge rate increases to 15 C, sample LFP7 has no discharge capacity, but samples LFP14 and LFP21 deliver discharge capacities of 92.9 and 90.5 mAh g^{-1}, respectively. It suggests that samples LFP14 and LFP21 are obviously better than sample LFP7, and sample LFP14 is the best among the three. Combined with the morphology and microstructure analysis of the samples,

the results reveal that appropriate carbon content with uniform carbon layer and moderate particle size with narrow distribution can enhance the electrochemical performance of LiFePO$_4$/C composites.

High rate performance is one of the significant electrochemical aspects of lithium ion batteries for high power applications (HEVs and EVs). Figure 5d further compares the rate capabilities and cycling performances of samples LFP7, LFP14, and LFP21. Rate capabilities of samples LFP7, LFP14, and LFP21 are evaluated from 0.1 C to 15 C and finally back to 0.1 C in the voltage range of 2.5–4.2 V; and ten cycles are performed at a given rate. Sample LFP7 delivers an initial discharge capacity of 150.5 mAh g^{-1} at 0.1 C and hardly presents discharge capacity when the discharge rate increases to 3 C. In addition, the storage capacity of sample LFP7 is not stable in each rate. Upon decreasing the current rate from 3 C to 0.1 C, a discharge capacity of 133.5 mAh g^{-1} is recovered, which is only 88.7 % of its initial capacity. As expected, samples LFP14 and LFP21 have excellent rate capabilities and cycling performances. The discharge capacities of samples LFP14 and LFP21 decrease from 158.8 and 154.1 mAh g^{-1} to 92.9 and 90.5 mAh g^{-1} with increasing current rate from 0.1 to 15 C, respectively. When decreasing the current rate from 15 C back to 0.1 C, the discharge capacities of 157.5 and 152.3 mAh g^{-1} are recovered, which are 99.2 % and 98.8 % of their initial capacities, respectively. Coating appropriate amount of carbon on

Fig. 5 Initial charge–discharge profiles of samples LFP7 (**a**), LFP14 (**b**), and LFP21 (**c**) at different discharge rates; comparison of the cycling performances of the three LiFePO$_4$/C composite samples (**d**)
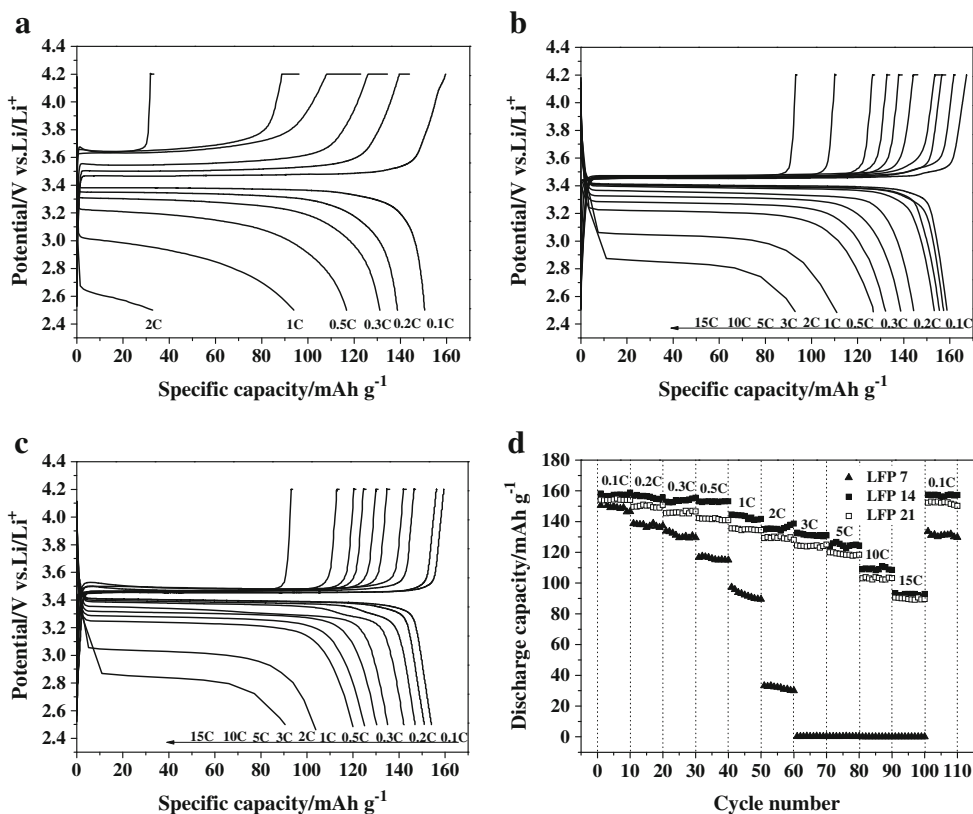
LiFePO$_4$ particles can improve the high rate performance and cycling performance because the coated carbon can not only enhance the electronic conductivity of LiFePO$_4$ but also prevent LiFePO$_4$ from dissolving by HF which may result from electrolyte decomposition (LiPF$_6$/EC + DMC as the electrolyte in the testing cell) [29]. The particle size and electrochemical polarization can be reduced effectively when LiFePO$_4$ particle surface is coated uniformly by conductive carbon. The discharge capacities of sample LFP14 can reach 158.8, 144.3, 111.0, and 92.9 mAh g^{-1} at 0.1, 1, 10, and 15 C respectively, which are the best among the three samples (LFP7, LFP14 and LFP21). Figure 6 presents the cycling performance of sample LFP14 at 0.5 C and shows that the discharge capacities of sample LFP14 are very stable after 100 cycles at 0.5 C.

In order to clarify the influence of structure and morphology of different Fe (III) raw materials, commercial Fe$_2$O$_3$ instead of β-FeOOH nanorods was used as Fe (III) source. Fe$_2$O$_3$ was used to compensate the same adding amount of iron source from β-FeOOH nanorods in sample LFP14. The sample synthesized using Fe$_2$O$_3$ as a Fe (III) raw material is denoted as LFP$_{Fe2O3}$. Fig. S2 shows the XRD patterns of sample LFP$_{Fe2O3}$ and all the diffraction peaks can be identified as LiFePO$_4$ (JCPDS card No. 83-2092). No impurities are detected in the XRD pattern. The particle size of sample LFP$_{Fe2O3}$ is about 500 nm–1.2 μm (Fig. S1f) and the carbon content is 2.76 wt.%, a little less carbon content than sample LFP14, but sample LFP$_{Fe2O3}$ has larger particle size than sample LFP14 and sample LFP7. In addition, sample LFP$_{Fe2O3}$ has the widest particle size distribution among all the samples. It suggests that the structure and the morphology of β-FeOOH nanorods can be helpful for minimizing the particle size and distribution of the final LiFePO$_4$/C material. The electrochemical properties of sample LFP$_{Fe2O3}$ are also given (as shown in Fig. S3). Initial charge–discharge profiles of sample LFP$_{Fe2O3}$ at different rates are shown in Fig. S3a. At 0.1 C rate, the discharge capacity of sample LFP$_{Fe2O3}$ (120.0 mAh g^{-1}) is lower than that of sample LFP14 (158.8 mAh g^{-1}) and sample LFP7

(150.5 mAh g^{-1}), and rate capability of sample LFP$_{Fe2O3}$ is poorer (as shown in Fig. S3b). The results show that the structure and the morphology of raw materials have effect on the morphology and electrochemical performance of the final product LiFePO$_4$/C.

Cyclic voltammetry was also carried out to investigate the effect of carbon coating and particle size on electrochemical properties of the LiFePO$_4$/C samples. As for cyclic voltammogram, the separation potential between anodic peak and cathodic peak is an important parameter to evaluate the electrochemical reaction reversibility. Figure 7 shows the CV profiles of samples LFP7, LFP10, LFP14, LFP17, and LFP21 at a scanning rate of 0.1 mV s^{-1} between 2.5 and 4.2 V. Sample LFP14 has the most symmetrical and spiculate shape of peak profile and the smallest value of potential interval among the five samples, which indicates that sample LFP14 has the best electrochemical reaction reversibility during lithium ion insertion and extraction.

EIS is an important method to evaluate the diffusion coefficient of lithium ion and is used to investigate the influence of carbon content and particle size on the lithium ions transfer in the LiFePO$_4$/C composite samples. The EIS measurements were carried out in the frequency range from 100 kHz to 10 mHz with an AC voltage signal of ±5 mV at room temperature. Figure 8a shows the Nyquist plot in the open circuit state with varying carbon contents at room temperature. An intercept at the real axis Z_{re} in high frequency corresponds to the ohmic resistance (R_e), which represents the resistance of the electrolyte, the semicircle in the middle frequency range indicates the charge transfer resistance (R_{ct}). The inclined line in the low-frequency represents the Warburg impedance (Z_w), which is associated with lithium ion diffusion in the LiFePO$_4$ particles.

A simplified Randles equivalent circuit model [30] (shown in the inset of Fig. 8a) is constructed to analyze the impedance spectra. A constant phase element is placed to represent the double layer capacitance and passivation film capacitance. As shown in Fig. 8a, the calculated values
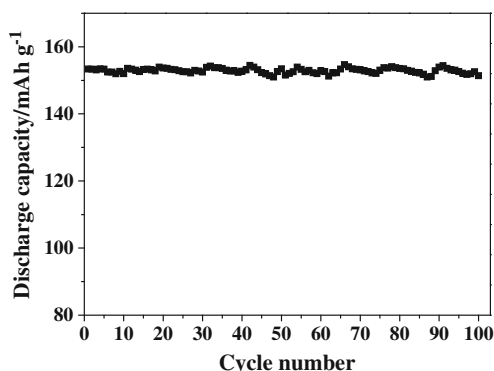

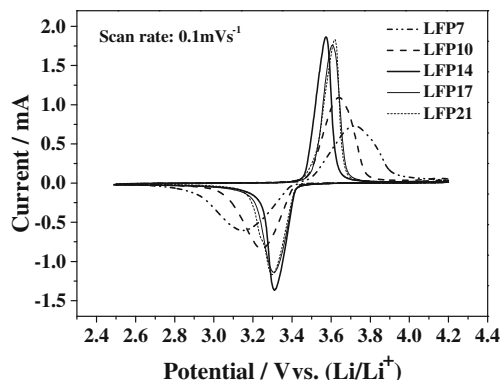Fig. 6 Cycling performance of sample LFP14 at 0.5 C between 2.5 and 4.2 V

Fig. 7 Cyclic voltammograms of samples LFP7, LFP10, LFP14, LFP17, and LFP21 at a scan rate of 0.1 mV s^{-1} between 2.5 and 4.2 V

Fig. 8 Comparison of the measured Nyquist plot and the calculated values (shown by the line) with the equivalent circuit shown in the figure (**a**); the relationship between Z_{re} and $\omega^{-1/2}$ at low frequency (**b**)
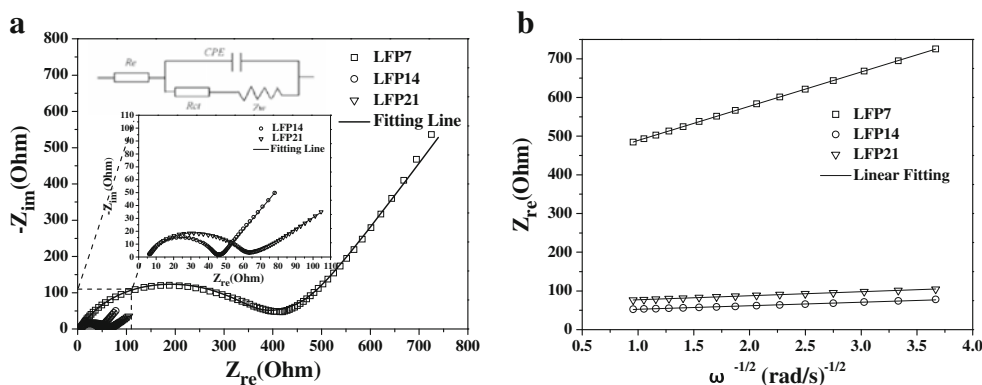
fit well with the measured values. The parameters of the equivalent circuit by computer simulation are shown in Table 1. Obviously, the ohmic resistances (R_e) are similar, but the charge transfer resistances (R_{ct}) decrease firstly and then increase a little with the increase of carbon content in the samples, which is ascribe to their differences in particle sizes and carbon coating. As shown in Fig. 3, sample LFP7 (Fig. 3a, b) has the largest particle sizes and has not enough carbon to coat all over particles. Sample LFP14 (Fig. 3e, f) has a comparatively more uniform particle size distribution and a smaller particle size. Meanwhile, it has enough carbon to coat all over the particles with uniform carbon layer. As for sample LFP21 (Fig. 3i,j), although the particle size distribution and particle size are similar to sample LFP14 and the active materials are also coated completely by carbon, the coated carbon layer is thick and rough. It is known that carbon coating and particle minimization are very useful to decrease R_{ct}, which leads to the enhancement of electrochemical performance of materials. However, when the particle size distribution and particle size are similar, the excessive carbon may increase R_{ct} [31]. As shown in Table 1, the charge transfer resistances (R_{ct}) of samples LFP7, LFP14, and LFP21 are 341.50, 37.74, and 49.97 Ω, respectively. As expected, sample LFP14 with a carbon content of 2.79 wt.% has the least R_{ct}. Combined with the electrochemical performance above, it is believed that decrease of charge transfer resistance is beneficial to the kinetic behaviors during charge–discharge process, thus leading to the improvement of electrochemical performance of materials.

The lithium ion diffusion coefficient (D) is calculated according to the following equation:

$$D = R^2 T^2 / 2A^2 n^4 F^4 C^2 \sigma^2 \tag{1}$$

where n is the number of electrons per molecule during oxidization, A is the surface area of the cathode, D is the diffusion coefficient of lithium ion, R is the gas constant, T is the absolute temperature, F is the Faraday constant, C is the concentration of lithium ion, and σ is the Warburg factor which has a relationship with Z_{re}:

$$Z_{re} = R_e + R_{ct} + \sigma \omega^{-1/2} \tag{2}$$

The $Z_{re}-\omega^{-1/2}$ plots of different samples are presented in Fig. 8b. The graph of Z_{re} against square root of frequency ($\omega^{-1/2}$) in the low-frequency region is a straight line with the slope of σ (the values are listed in Table 1). The diffusion coefficients of lithium ion calculated based on Eqs. (1) and (2) are also listed in Table 1. The calculated diffusion coefficients (D) of samples LFP7, LFP14, and LFP21 are 8.46×10^{-14}, 7.69×10^{-12}, and 6.19×10^{-12} cm^2/s, respectively. It suggests that the low Li ion diffusion rate can be overcome through reducing the particle size and coating appropriate amount of carbon. Sample LFP14 has the least charge transfer resistance ($R_{ct}=37.740$ Ω) and the highest diffusion coefficient ($D=7.69\times10^{-12}$ cm^2/s), which are consistent with its excellent electrochemical performance.

Conclusions

In this paper, we have successfully prepared LiFePO$_4$/C composites via a carbothermal reduction method using uniform β-FeOOH nanorods as raw materials and glucose as both reducing agent and carbon source. The content of carbon and the morphology of raw material have an effect on electrochemical performance of final LiFePO$_4$/C material. The results indicate that LiFePO$_4$/C composite with a carbon content of about 2.79 wt.% (sample LFP14) can offer an excellent electrochemical performance. It can

Table 1 The resistances, Warburg factors, and diffusion coefficients of samples LFP7, LFP14, and LFP21

Sample	R_e (Ω)	R_{ct} (Ω)	σ (Ω s$^{1/2}$)	D (cm^2/s)
LFP7	5.957	341.500	88.573	8.46×10^{-14}
LFP14	5.916	37.740	9.2910	7.69×10^{-12}
LFP21	5.943	49.970	10.359	6.19×10^{-12}

deliver a discharge capacity of 158.8 mAh g^{-1} at 0.1 C and 92.9 mAh g^{-1} even at the discharge rate up to 15 C. When decreasing the current rate from 15 C back to 0.1 C, a discharge capacity of 157.5 mAh g^{-1} is recovered, which is 99.2 % of its initial capacity. In addition, it exhibits a good cycling performance and shows little degradation after 100 cycles at 0.5 C. Such an excellent rate and cycling performance can be attributed to its fine particle size which can facilitate fast electrochemical reaction kinetics, and even coated carbon layer which not only enhances the electronic conductivity of LiFePO$_4$ but also prevents LiFePO$_4$ from HF etching to some extent. This method could provide a useful route for industrial preparation of LiFePO$_4$ cathode materials to satisfy the needs in HEVs, EVs, and other mobile or portable electric devices.

References

1. Tarascon JM, Armand M (2001) Issues and challenges facing rechargeable lithium batteries. Nature 414:359–367
2. Armand M, Tarascon JM (2008) Building better batteries. Nature 451:652–657
3. Bruce PG, Scrosati B, Tarascon JM (2008) Nanomaterials for rechargeable lithium batteries. Angew Chem Int Ed 47:2930–2946
4. Padhi AK, Nanjundaswamy KS, Goodenough JB (1997) Phospho-olivines as positive-electrode materials for rechargeable lithium batteries. J Electrochem Soc 144:188–1194
5. Chung SY, Bloking JT, Chiang YM (2002) Electronically conductive phospho-olivines as lithium storage electrodes. Nat Mater 1:123–128
6. Ravet N, Chouinard Y, Magnan JF et al (2001) Electroactivity of natural and synthetic triphylite. J Power Sources 97–98:503–507
7. Pei B, Wang Q, Zhang WX et al (2011) Enhanced performance of LiFePO$_4$ through hydrothermal synthesis coupled with carbon coating and cupric ion doping. Electrochim Acta 56:5667–5672
8. Liu H, Cao Q, Fu LJ et al (2006) Doping effects of zinc on LiFePO$_4$ cathode material for lithium ion batteries. Electrochem Commun 8:1553–1557
9. Yang MR, Ke WH (2008) The doping effect on the electrochemical properties of LiFe$_{0.95}$M$_{0.05}$PO$_4$ (M=Mg^{2+}, Ni^{2+}, Al^{3+}, or V^{3+}) as cathode materials for lithium-ion cells. J Electrochem Soc 155:A729–A732
10. Wang YQ, Wang JL, Yang J et al (2006) High-rate LiFePO$_4$ electrode material synthesized by a novel route from FePO$_4$·4H$_2$O. Adv Funct Mater 16:2135–2140
11. Yamada A, Chung SC, Hinokuma K (2001) Optimized LiFePO$_4$ for lithium battery cathodes. J Electrochem Soc 148:A224–A229
12. Yu DYW, Donoue K, Inoue T et al (2006) Effect of electrode parameters on LiFePO$_4$ cathodes. J Electrochem Soc 153:A835–A839
13. Wang Y, Sun B, Park J et al (2011) Morphology control and electrochemical properties of nanosize LiFePO$_4$ cathode material synthesized by co-precipitation combined with in situ polymerization. J Alloys Compd 509:1040–1044
14. Lu CZ, Fey GTK, Kao HM (2009) Study of LiFePO$_4$ cathode materials coated with high surface area carbon. J Power Sources 189:155–162
15. Jamnik J, Dominko R, Erjavec B et al (2009) Stabilizers of particle size and morphology: a road towards high-rate performance insertion materials. Adv Mater 21:2715–2719
16. Choi D, Kumta PN (2007) Surfactant based sol-gel approach to nanostructured LiFePO$_4$ for high rate Li-ion batteries. J Power Sources 163:1064–1069
17. Yu F, Zhang JJ, Yang YF et al (2010) Porous micro-spherical aggregates of LiFePO$_4$/C nanocomposites: A novel and simple template-free concept and synthesis via sol-gel-spray drying method. J Power Sources 195:6873–6878
18. Dokko K, Koizumi S, Nakano H et al (2007) Particle morphology, crystal orientation, and electrochemical reactivity of LiFePO$_4$ synthesized by the hydrothermal method at 443 K. J Mater Chem 17:4803–4810
19. Yang M, Gao QM (2011) LiFePO$_4$/C composite cathode material with a continuous porous carbon network for high power lithium-ion battery. J Alloys Compd 509:3690–3698
20. Kim DK, Park HM, Jung SJ et al (2006) Effect of synthesis conditions on the properties of LiFePO$_4$ for secondary lithium batteries. J Power Sources 159:237–240
21. Kim HS, Kam DW, Kim WS et al (2011) Synthesis of the LiFePO$_4$ by a solid-state reaction using organic acids as a reducing agent. Ionics 17:293–297
22. Kim JK, Cheruvally G, Choi JW et al (2007) Effect of mechanical activation process parameters on the properties of LiFePO$_4$ cathode material. J Power Sources 166:211–218
23. Kang HC, Jun DK, Jin B et al (2008) Optimized solid-state synthesis of LiFePO$_4$ cathode materials using ball-milling. J Power Sources 179:340–346
24. Ren JG, Pu WH, He XM et al (2011) A carbon-LiFePO$_4$ nanocomposite as high-performance cathode material for lithium-ion batteries. Ionics 17:581–586
25. Wang YG, Wang YR, Hosono E et al (2008) The design of a LiFePO$_4$/Carbon nanocomposite with a core-shell structure and its synthesis by an in situ polymerization restriction method. Angew Chem Int Ed 47:1–6
26. Yang LM, Liang GC, Wang L et al (2010) Effect of consumption amount of lithium salt on the properties of LiFePO$_4$/C cathode materials. J Alloys Compd 496:376–379
27. Sun LQ, Cui RH, Jalbout AF et al (2009) LiFePO$_4$ as an optimum power cell material. J Power Sources 189:522–526
28. Yang GL, Zhang XF, Liu J et al (2010) Synthesis of LiFePO$_4$/polyacenes using iron oxyhydroxide as an iron source. J Power Sources 195:1211–1215
29. Zhi XK, Liang GC, Wang L et al (2009) The cycling performance of LiFePO$_4$/C cathode materials. J Power Sources 189:779–782
30. Gao F, Tang ZY (2008) Kinetic behavior of LiFePO$_4$/C cathode material for lithium-ion batteries. Electrochim Acta 53:5071–5075
31. Zhi XK, Liang GC, Wang L et al (2010) Optimization of carbon coatings on LiFePO$_4$: carbonization temperature and carbon content. J Alloys Compd 503:370–374